

Controllable Emergence of Multiple Topological Anderson Insulator Phases in Photonic Su-Schrieffer-Heeger Lattices

Ruijiang Ji,¹ Yunbo Zhang,^{2,*} Shu Chen,^{3,4,†} and Zhihao Xu^{1,5,‡}

¹*Institute of Theoretical Physics and State Key Laboratory of Quantum Optics Technologies and Devices, Shanxi University, Taiyuan 030006, China*

²*Zhejiang Key Laboratory of Quantum State Control and Optical Field Manipulation, Department of Physics, Zhejiang Sci-Tech University, Hangzhou 310018, China*

³*Beijing National Laboratory for Condensed Matter Physics,*

Institute of Physics, Chinese Academy of Sciences, Beijing 100190, China

⁴*School of Physical Sciences, University of Chinese Academy of Sciences, Beijing 100049, China*

⁵*Collaborative Innovation Center of Extreme Optics, Shanxi University, Taiyuan 030006, China*

(Dated: December 9, 2025)

We investigate the emergence and control of multiple topological Anderson insulator (TAI) phases in a one-dimensional Su-Schrieffer-Heeger (SSH) waveguide lattice with generalized Bernoulli-type disorder introduced in the intradimer couplings. By systematically varying the disorder configuration—including the values and probabilities of the multivariate distribution—we demonstrate that both the number and width of TAI phases can be precisely engineered. Analytical determination of topological phase boundaries via the inverse localization length shows excellent agreement with numerical simulations. Our results reveal a rich landscape of disorder-induced topological phase transitions, including multiple reentrant TAI phases that arise as the disorder amplitude increases. Furthermore, we show that the mean chiral displacement serves as a sensitive probe for detecting these topological transitions, providing a practical route for experimental realization in photonic waveguide lattices. This work establishes a versatile framework for designing quantum and photonic materials with customizable topological properties driven by tailored disorder.

Introduction.—Topological photonics is a rapidly developing field at the intersection of condensed matter physics and photonic engineering, offering new ways to manipulate light through topological concepts^{1,2}. By leveraging principles originally developed for electronic systems, photonic platforms can support robust edge states and topologically protected transport, resilient to disorder and fabrication imperfections. This has enabled transformative applications including disorder-resistant waveguides^{3–5}, robust photonic circuits⁶, topological lasers^{7–9}, and programmable photonic chips^{10,11}, with promising prospects for integrated photonics and quantum information technologies.

A key challenge is the precise and controllable realization of topological phases. Tunable topological states not only advance fundamental physics but also enable photonic devices with customizable functions, such as reconfigurable logic and topologically protected routing¹². Among various approaches, disorder-induced topological phases^{13–28}—especially the topological Anderson insulator (TAI)^{29–44}—have attracted considerable interest, showing that disorder can induce and stabilize topological phenomena. TAIs have been realized in diverse systems, from one-dimensional (1D) cold atomic wires⁴⁵ and 2D photonic arrays^{5,46} to photonic quantum walks³⁹. Beyond Anderson-type disorder, quasiperiodic and other structured disorders can also drive TAI transitions^{47–55}. Notably, modulated or structured disorder can induce multiple distinct TAI phases, each with unique topological transitions^{52,56}.

Despite this progress, engineering and controlling multiple topological phases within a single photonic plat-

form remains challenging. Here, we propose a versatile scheme for the controllable emergence of multiple TAI phases in photonic Su-Schrieffer-Heeger (SSH) lattices. Specifically, we investigate a 1D SSH waveguide lattice with generalized Bernoulli-type disorder in the intradimer couplings, enabling multiple TAI phases to arise from an initially trivial band structure. By tuning the hopping amplitude and disorder strength, we observe a sequence of topological phase transitions, including the robust persistence of nontrivial phases at weak disorder, and the emergence of multiple TAI phases at larger amplitudes. The configuration of the disorder—set by the values and probabilities in the generalized Bernoulli distribution—allows precise control over the number and width of TAI intervals. Our model is experimentally accessible in photonic waveguide lattices, where topological transitions can be detected via mean chiral displacement. These results provide a tunable framework for engineering quantum and photonic materials with customizable topological properties.

Model and method.—We consider a 1D array of optical waveguides with tailored coupling constants. When the spacing between adjacent waveguides alternates, the resulting structure realizes the SSH model, which is known to exhibit a topological Anderson phase transition in the presence of uncorrelated disorder⁴⁵. In the absence of disorder, the SSH model features two topologically distinct phases, characterized by the topological invariant $Q = 0$ for $t_1 > t_2$ and $Q = 1$ for $t_1 < t_2$, where t_1 and t_2 denote the intra- and interdimer hopping amplitudes, respectively. In this work, we investigate an SSH chain with uniform interdimer hopping t_2 , while introducing a gen-

eralized Bernoulli-type modulation ξ_i to the intradimer hopping t_1 . The light propagation in the waveguide array is governed by coupled-mode equations:

$$\begin{aligned} i \frac{dc_{i,A}}{dz} &= -(t_1 - \xi_i)c_{i,B} - t_2 c_{i-1,B}, \\ i \frac{dc_{i,B}}{dz} &= -(t_1 - \xi_i)c_{i,A} - t_2 c_{i+1,A}, \end{aligned} \quad (1)$$

where $c_{i,\sigma}$ denote the mode amplitude on sublattice site $\sigma = A, B$ in the i -th unit cell, and the propagation axis z serves as an effective time variable. The generalized Bernoulli-type disorder ξ_i in the i -th unit cell is defined as a multivariate distribution with M possible values, namely $\xi^{(1)}, \xi^{(2)}, \dots, \xi^{(M)}$, occurring with probabilities p_1, p_2, \dots, p_M , respectively, such that $\sum_j p_j = 1$. Accordingly, ξ_i is drawn from a multi-modal probability distribution function, $P(\xi_i) = \sum_{j=1}^M p_j \delta(\xi_i - \xi^{(j)})$, meaning that ξ_i takes the value $\xi^{(j)}$ with probability p_j in i -th unit cell. The required Bernoulli-type modulation can be implemented by controlled fabrication of discrete coupling distances. The light propagation in the waveguide array can also be described by an effective tight-binding Hamiltonian:

$$\hat{H} = \sum_i \left[-(t_1 - \xi_i) \hat{c}_{i,A}^\dagger \hat{c}_{i,B} - t_2 \hat{c}_{i,B}^\dagger \hat{c}_{i+1,A} + H.c. \right], \quad (2)$$

where $\hat{c}_{i,\sigma}$ ($\hat{c}_{i,\sigma}^\dagger$) is the annihilation (creation) operator for a particle on the sublattice σ of the i -th unit cell. For convenience, we set $t_2 = 1$ as the unit energy throughout our discussion.

Owing to the chiral symmetry of our modulated SSH model, which satisfies $\Gamma \hat{H} = -\hat{H} \Gamma$, where the chiral symmetry operator is defined as $\Gamma = I_N \otimes \sigma_z$, with σ_z being the Pauli z -matrix, I_N the $N \times N$ identity matrix, and N the number of unit cells, we employ the topological invariant Q to characterize the topological states. This topological invariant is constructed from the reflection matrix and enumerates the number of robust bound states at the ends⁵⁷. Notably, the topological invariant Q remains well-defined even in systems lacking translational symmetry, which reads

$$Q = \frac{1}{2} \left(1 - \text{sgn} \left[\prod_i (-t_1 + \xi_i)^2 - \prod_i (-t_2)^2 \right] \right). \quad (3)$$

For $Q = 1$, nontrivial zero modes emerge and localize at both edges of the chain, indicating a topologically nontrivial phase. Conversely, when $Q = 0$, the absence of zero modes corresponds to a topologically trivial phase. To account for the effect of randomness, we further define the disorder-averaged topological invariant $\overline{Q} = 1/N_c \sum_{c=1}^{N_c} Q_c$, where N_c is the number of the disorder realizations and Q_c is the topological invariant for the c -th realization. This averaging procedure can effectively eliminate the influence of random fluctuations.

In the topologically nontrivial phase, the zero modes are localized at the edges of the chain with a finite localization length. However, as the system transitions into

the trivial phase, these zero-mode edge states vanish and bulk states dominate, accompanied by the emergence of a divergence of the localization length⁵⁸. Consequently, the topological phase boundaries can be analytically determined by examining the inverse localization length γ of the zero modes. The Schrödinger equation for the zero modes in our modulated SSH model, $\hat{H}|\psi\rangle = 0$, can be written as

$$\begin{aligned} (-t_1 + \xi_i) \psi_{i,B} - t_2 \psi_{i-1,B} &= 0, \\ (-t_1 + \xi_i) \psi_{i,A} - t_2 \psi_{i+1,A} &= 0, \end{aligned} \quad (4)$$

where $\psi_{i,\sigma}$ denotes the probability amplitude of the zero mode on sublattice site σ in the i -th lattice cell. By solving these coupled equations, one obtains $\psi_{N+1,A} = (-1)^N \prod_{i=1}^N [(-t_1 + \xi_i)/(-t_2)] \psi_{1,A}$, leading to the inverse localization length for the zero modes,

$$\begin{aligned} \gamma &= -\lim_{N \rightarrow \infty} \frac{1}{N} \ln \left| \frac{\psi_{N+1,A}}{\psi_{1,A}} \right| \\ &= \lim_{N \rightarrow \infty} \left(\ln |t_2| + \ln \left| \left[\prod_{j=1}^M \left(-t_1 + \xi^{(j)} \right)^{l_j/N} \right]^{-1} \right| \right) \\ &= \ln |t_2| + \ln \left| \left[\prod_{j=1}^M \left(-t_1 + \xi^{(j)} \right)^{p_j} \right]^{-1} \right|, \end{aligned} \quad (5)$$

where l_j is the number of occurrences of the value $\xi^{(j)}$ in N unit cells, and $\sum_j l_j = N$. The topological phase boundaries can be determined by the condition $\gamma = 0$, yielding

$$\left| \prod_{j=1}^M \left(-t_1 + \xi^{(j)} \right)^{p_j} \right| = 1. \quad (6)$$

It is evident that, once the specific values of $\xi^{(j)}$ and p_j are given, the phase transition boundaries can be precisely determined.

Tunable Multiple TAI Phases.—We begin by considering the case of binary modulation, which corresponds to an SSH model with standard Bernoulli-type disorder. Figure 1(a) presents the disorder-averaged topological phase diagram as a function of t_1 and λ , where $\xi^{(1)} = \lambda$ and $\xi^{(2)} = 2\lambda$ occur with probabilities $p_1 = 2/5$ and $p_2 = 3/5$, respectively. The results are obtained by numerically calculating the disorder-averaged topological invariant \overline{Q} over $N_c = 200$ disorder realizations. In the absence of modulation ($\lambda = 0$), the system exhibits a topological phase transition at $t_1 = 1$, corresponding to a sharp drop in \overline{Q} from 1 to 0 as t_1 increases. When disorder is introduced into the nontrivial regime ($0 < t_1 < 1$), the topologically nontrivial phase remains robust against weak disorder, but eventually transitions to a trivial phase as the disorder amplitude increases.

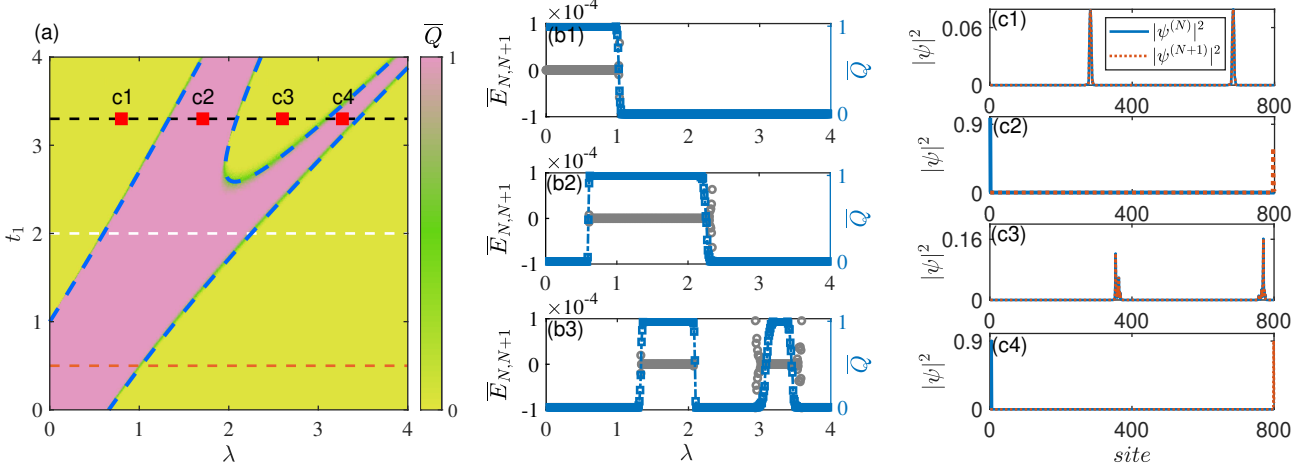


FIG. 1: (a) Topological phase diagram characterized by the disorder-averaged topological invariant \bar{Q} , as a function of intradimer hopping amplitude t_1 and disorder amplitude λ for $p_1 = 2/5$ and $p_2 = 3/5$. Orange, white, and black dashed lines indicate $t_1 = 0.5$, 2.0 , and 3.3 , respectively; blue dashed lines mark the analytical phase boundaries. (b1)-(b3) Disorder-average central energies \bar{E}_N , \bar{E}_{N+1} and topological number \bar{Q} versus λ under OBC for $t_1 = 0.5$, 2.0 , and 3.3 , respectively. (c1)-(c4) Density distributions of the N -th and $N + 1$ -th eigenstates under OBCs for $\lambda = 0.80$, 1.71 , 2.60 , and 3.27 (marked by red squares in (a)). All data averaged over $N_c = 200$ disorder realizations, $N = 400$ and $\xi^{(1)} = \lambda$, $\xi^{(2)} = 2\lambda$.

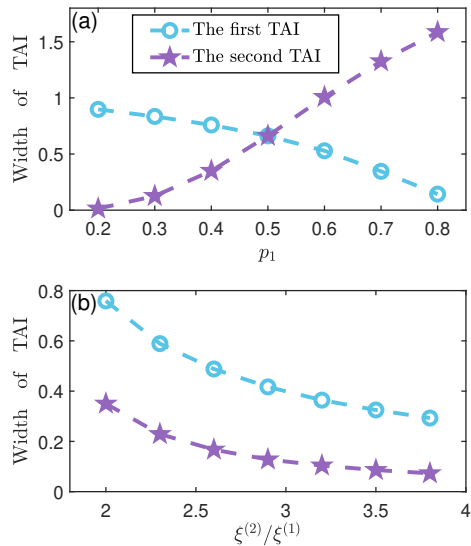


FIG. 2: (a) Widths of the first and second TAI phases as a function of probability distribution for $t_1 = 3.3$ with $\xi^{(1)} = \lambda$ and $\xi^{(2)} = 2\lambda$. (b) Widths of the first and second TAI phases versus $\xi^{(2)}/\xi^{(1)}$ for $t_1 = 3.3$ with $\xi^{(1)} = \lambda$, $p_1 = 2/5$, and $p_2 = 3/5$.

For $1.00 < t_1 < 2.59$, the system undergoes a sequence of topological phase transitions—from trivial to nontrivial and back to trivial—as λ increases, indicating the emergence of the TAI phase. When $t_1 > 2.59$, the system experiences two distinct transitions into the TAI phase before ultimately returning to a trivial phase at larger values of λ . According to Eq. (6), the phase boundaries are

delineated by the blue dashed lines, which follow the analytical condition $|(-t_1 + \lambda)^{2/5}(-t_1 + 2\lambda)^{3/5}| = 1$. These findings illustrate the intricate relationship between disorder and topological phases in the SSH model, highlighting how Bernoulli-type modulation can significantly influence the system's topological properties.

Figures 1(b1)-1(b3) display the disorder-averaged energies \bar{E}_N and \bar{E}_{N+1} , alongside the disorder-averaged topological invariant \bar{Q} , as functions of λ under open boundary conditions (OBCs) for $t_1 = 0.5$, 2.0 , and 3.3 , respectively. Here, $\bar{E}_n = 1/N_c \sum_{c=1}^{N_c} E_n^{(c)}$, where $E_n^{(c)}$ denotes the n -th eigenvalue for a given disorder configuration. For $t_1 = 0.5$ [Fig. 1(b1)], $\bar{Q} = 1$ and both \bar{E}_N and \bar{E}_{N+1} remain pinned at zero in the weak-disorder regime, and the system becomes trivial when $\lambda > 1$, indicating robustness of the nontrivial phase against weak disorder. For $t_1 = 2.0$ [Fig. 1(b2)], increasing λ drives a sequence of topological transitions from trivial to nontrivial and back to trivial; the TAI phase appears in the range $\lambda \in (0.60, 2.25)$, where $\bar{Q} = 1$ and two degenerate zero modes emerge. For $t_1 > 2.59$, exemplified by $t_1 = 3.3$ in Fig. 1(b3), \bar{Q} switches to a nontrivial value, corresponding to the emergence of zero modes in the intervals $\lambda \in (1.33, 2.09) \cup (3.10, 3.45)$. The system thus undergoes two transitions between trivial and nontrivial phases, indicating the presence of multiple TAI phases. Furthermore, Figs. 1(c1)-1(c4) present the density distributions of the N -th and $(N + 1)$ -th eigenstates, $|\psi^{(N)}|^2$ and $|\psi^{(N+1)}|^2$, for a single disorder realization under OBCs for $t_1 = 3.3$ with $\lambda = 0.80$, 1.71 , 2.60 , and 3.27 , respectively. In the topologically nontrivial regimes, both states are localized at the ends of the chain, whereas in the trivial regimes, they become localized bulk states. These density distributions further corroborate the emergence

of multiple TAI phases in the system. Overall, these results demonstrate that the interplay between Bernoulli-type modulation and hopping amplitudes leads to rich topological phase behavior, including multiple reentrant transitions and the robust emergence of the TAI phase.

Notably, we find that both the probability of the binary distribution of disorder and the ratio between its two values, $\xi^{(2)}/\xi^{(1)}$, play a crucial role in determining and tuning the parameter range over which the TAI phases emerge. In Fig. 2(a), we present the widths of the two TAI phases for $t_1 = 3.3$ as a function of p_1 , with $\xi^{(1)} = \lambda$ and $\xi^{(2)} = 2\lambda$. As the disorder amplitude λ increases in this binary modulated scenario, the two TAI phases emerge sequentially. With increasing probability p_1 of $\xi^{(1)}$, the width of the first TAI phase gradually narrows, while the width of the second TAI phase correspondingly broadens. For $p_1 < 1/2$, the width of the first TAI phase remains larger than that of the second; however, when $p_1 > 1/5$, the second TAI phase becomes wider than the first. In Fig. 2(b), we fix the probabilities of the binary distribution at $p_1 = 2/5$ and $p_2 = 3/5$, and plot the widths of the two TAI phases for $t_1 = 3.3$ as a function of $\xi^{(2)}/\xi^{(1)}$ with $\xi^{(1)} = \lambda$. As shown, both TAI phase widths decrease as $\xi^{(2)}/\xi^{(1)}$ increases, while the width of the first TAI phase consistently remains larger than that of the second across different values of $\xi^{(2)}/\xi^{(1)}$. Our results demonstrate that both the probability distribution and the ratio of values in the binary disorder play pivotal roles in shaping the phase diagram of the system. By tuning these parameters, one can effectively control not only the emergence but also the width of multiple TAI phases. This highlights the high degree of tunability and richness of topological phase transitions in systems with binary disorder modulation.

We next consider the cases where the disorder follows a multivariate distribution with $M > 2$. Figure 3(a) shows the disorder-averaged topological phase diagram as a function of t_1 and λ for $M = 3$, obtained by numerically averaging the disorder-averaged topological invariant \overline{Q} over $N_c = 200$ disorder realizations. In this scenario, we employ a trivariate distribution with $\xi^{(1)} = \lambda$, $\xi^{(2)} = 2\lambda$, and $\xi^{(3)} = 3\lambda$, occurring with probabilities $p_1 = 1/2$ and $p_2 = p_3 = 1/4$. In the region $t_1 < 1$, sufficiently strong disorder destroys the topologically nontrivial phase as before. For $1.00 < t_1 < 2.23$, the system undergoes a sequence of topological phase transitions from trivial to nontrivial and then back to trivial as λ increases, indicating the emergence of the TAI. When $t_1 > 2.23$, the system exhibits multiple distinct transitions into the TAI phase before eventually returning to a trivial phase at larger values of λ . For sufficient large t_1 , the number of TAI phase emergences matches the number of disorder components, $M = 3$. The phase boundaries are determined by Eq. (6), delineated by the blue dashed line, and follow the relation $|(-t_1 + \lambda)^{1/2}(-t_1 + 2\lambda)^{1/4}(-t_1 + 3\lambda)^{1/4}| = 1$. Figures 3(b1)-(b3) display the disorder-averaged energies of the two center modes, \overline{E}_N and \overline{E}_{N+1} , along with the topo-

logical invariant \overline{Q} as functions of λ for different values of t_1 . As shown in Fig. 3(b1) for $t_1 = 0.5$, the topologically nontrivial phase remains robust against weak disorder within the range $\lambda \in (0, 1)$, as indicated by the unit value of \overline{Q} and the presence of two degenerate zero-energy modes. However, with increasing disorder amplitude, the system undergoes a transition to a topologically trivial phase. For $t_1 = 2.0$, as shown in Fig. 3(b2), increasing λ drives the system through a sequence of topological phase transition: from trivial to nontrivial and then back to trivial. The nontrivial phase, identified as the TAI, emerges in the range $\lambda \in (0.5, 2.3)$, characterized by a unit value of \overline{Q} and the appearance of degenerate zero-energy modes. For $t_1 = 3.3$, as illustrated in Fig. 3(b3), the topological invariant \overline{Q} switches to a nontrivial value in the intervals $\lambda \in (1.05, 1.18) \cup (1.53, 1.76) \cup (3.06, 3.50)$, corresponding to the emergence of zero modes. The system thus undergoes three distinct transitions from trivial to nontrivial phases, indicating the appearance of multiple TAI phases.

The probability distribution and the specific values within the multivariate disorder are crucial in shaping the parameter space in which TAI phases can be realized. Figure 3(c) illustrates how the widths of the three TAI phases for $t_1 = 3.3$ vary as a function of p_2 , with $p_1 = 1/2$ held constant and $\xi^{(1)} = \lambda$, $\xi^{(2)} = 2\lambda$, and $\xi^{(3)} = 3\lambda$. As the disorder amplitude λ increases in this trivariate scenario, the three TAI phases emerge sequentially. Detailed analysis reveals that increasing the probability p_2 for $\xi^{(2)}$ causes the first TAI phase to narrow progressively, while the second and third phases expand in width. Specifically, for $p_2 < 0.215$, the first TAI phase is wider than the second; when $p_2 > 0.215$, the second TAI phase becomes dominant in width over the first. This demonstrates that by tailoring the probabilities of the disorder components, one can precisely manipulate the relative extent of multiple TAI phases within the system. Figure 3(d) further investigates the impact of the relative amplitudes of the disorder components on the widths of the TAI phases. Here, the probabilities are fixed at $p_1 = 1/2$ and $p_2 = p_3 = 1/4$, while the widths of the three TAI phases for $t_1 = 3.3$ are plotted as a function of $\xi^{(2)}/\xi^{(1)}$ with $\xi^{(1)} = \lambda$ and $\xi^{(3)} = 3\lambda$. The results show that as $\xi^{(2)}/\xi^{(1)}$ increases, the width of the first TAI phase grows, the width of the third TAI phase diminishes, and the second TAI phase exhibits a non-monotonic trend—first narrowing, then broadening. Throughout the entire range of $\xi^{(2)}/\xi^{(1)}$, the third TAI phase consistently possesses the greatest width, followed by the second and then the first TAI phase. These findings underscore the sensitive dependence of the TAI phase structure on both probability and the relative amplitudes of disorder component in trivariate distributions.

In Appendix, we display the disorder-averaged topological phase diagrams as functions of t_1 and λ for $M = 4$ and $M = 5$. The overall structure of the topological phase diagrams for $M = 4$ and $M = 5$ remains similar to those observed for $M = 2$ and 3 . Notably, in the regime

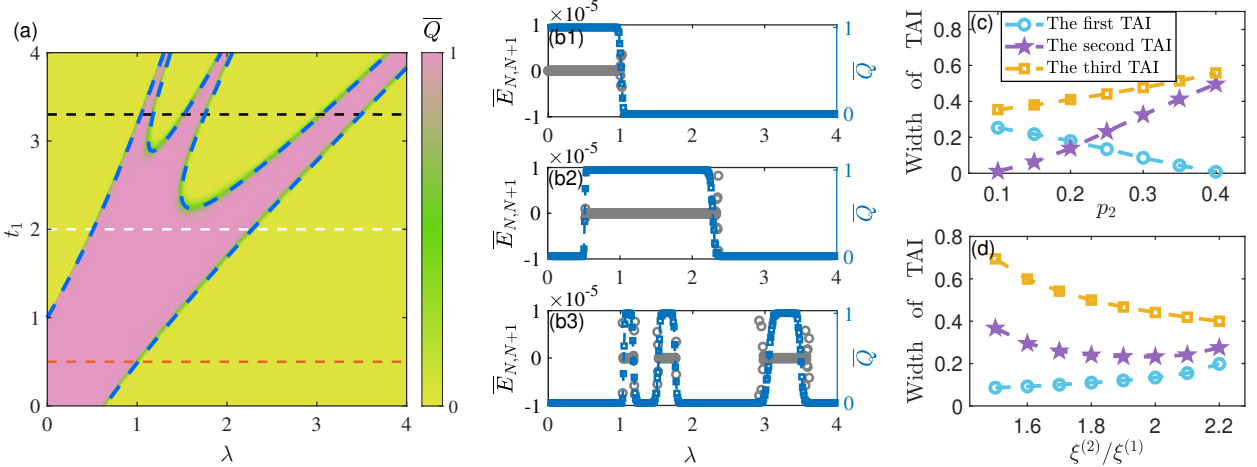


FIG. 3: (a) Topological phase diagram characterized by the disorder-averaged topological invariant \bar{Q} , as a function of intradimer hopping t_1 and disorder amplitude λ ($p_1 = 1/2$, $p_2 = p_3 = 1/4$). Orange, white, and black dashed lines indicate $t_1 = 0.5$, 2.0, and 3.3; blue dashed lines mark analytical phase boundaries. (b1)-(b3) Disorder-averaged central energies \bar{E}_N , \bar{E}_{N+1} , and topological number \bar{Q} versus λ under OBC for $t_1 = 0.5$, 2.0, and 3.3, respectively. (c) Widths of TAI phases for different p_2 ($\xi^{(1)} = \lambda$, $\xi^{(2)} = 2\lambda$, $\xi^{(3)} = 3\lambda$, $p_1 = 1/2$). (d) Widths of TAI phases versus $\xi^{(2)}/\xi^{(1)}$ ($\xi^{(1)} = \lambda$, $\xi^{(3)} = 3\lambda$, $p_1 = 1/2$, $p_2 = p_3 = 1/4$). All data averaged over $N_c = 200$ disorder realizations, and $N = 400$.

of large t_1 , the number of TAI phase emergences increases with the value of M , reflecting the direct influence of disorder complexity on the richness of topological behavior. These results further demonstrate that the multivariate nature of the disorder provides a powerful means to engineer and control multiple TAI phases within the system.

Dynamical detection.—Waveguide lattices are versatile platforms in integrated photonics, allowing exploration of crystalline-like phenomena and precise engineering of disordered systems^{3,59–62}. In previous section, we have shown that by engineering intradimer Bernoulli-type disorder in a 1D SSH waveguide lattice, multiple TAI phases can be realized. To probe the system’s topology in a dynamical and experimentally accessible way, we employ the mean chiral displacement, defined as

$$\bar{C}(t) = \frac{2}{N_c} \sum_{c=1}^{N_c} \langle \Gamma X \rangle_c \quad (7)$$

where Γ is the chiral symmetry operator, X is the unit-cell position operator, and $\langle \dots \rangle_c$ denotes the time-dependent expectation value for the c -th disorder realization^{51,63,64}. The validity of $\bar{C}(t)$ as a topological probe is supported by previous theoretical and experimental works on 1D chiral-symmetric systems, which show that in the long-time limit the (disorder-)averaged mean chiral displacement converges to the bulk winding number, and remains quantized even in the presence of disorder and localization^{45,63,64}. In our model, as shown in Figs. 4(a) and 4(c), $\bar{C}(t)$ approaches zero in the topologically trivial phase and unity in the nontrivial phase⁴⁵. To obtain a clearer phase signature, we consider the time-averaged mean chiral displacement, $\langle \bar{C} \rangle$, which converges to one for topologically nontrivial phases and to zero for

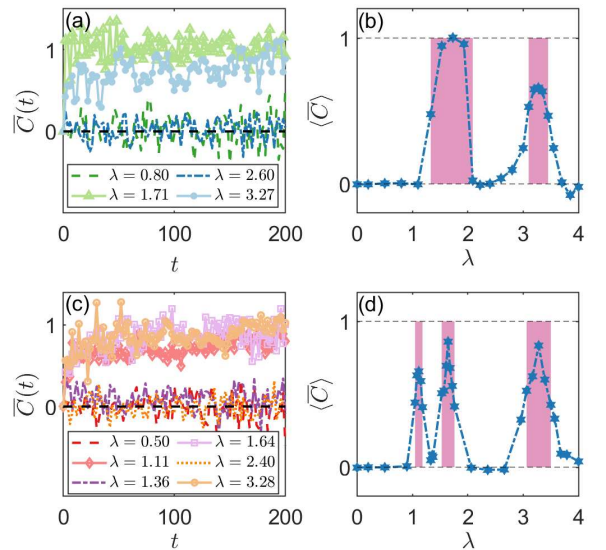


FIG. 4: Disorder-averaged mean chiral displacement operator $\bar{C}(t)$ versus time t for various disorder amplitudes λ ($N = 200$ and $N_c = 300$) for (a) $M = 2$ and (c) $M = 3$. Time-averaged chiral displacement $\langle \bar{C} \rangle$ as a function of λ ($N = 100$ and $N_c = 300$), averaged over time steps from 0 to 100 (step size 0.5), for (b) $M = 2$ and (d) $M = 3$. The pink regions indicate topologically nontrivial phase. Parameters: (a), (b) $\xi^{(1)} = \lambda$, $\xi^{(2)} = 2\lambda$, $p_1 = 2/5$, $p_2 = 3/5$; (c), (d) $\xi^{(1)} = \lambda$, $\xi^{(2)} = 2\lambda$, $\xi^{(3)} = 3\lambda$, $p_1 = 1/2$, $p_2 = p_3 = 1/4$.

trivial ones. Figures 4(b) and 4(d) show that as λ increases, $\langle \bar{C} \rangle$ starts at zero, then exhibits discrete jumps to nontrivial values—twice in Fig. 4(b) and three times

in Fig. 4(d)—before eventually returning to zero. These results clearly demonstrate that the mean chiral displacement serves as a sensitive and effective probe for detecting multiple TAI phases and the associated topological transitions induced by disorder amplitude in our model.

Conclusion.—We have systematically investigated the emergence and tunability of multiple TAI phases in a 1D SSH model with generalized Bernoulli-type disorder. By introducing a multivariate distribution to the intradimer hopping amplitudes, we demonstrated that both the probability distribution and the specific values of the disorder components play pivotal roles in shaping the topological phase diagram. Our results reveal that the number and width of TAI phases can be precisely controlled by tuning the parameters of the disorder, providing a versatile platform for engineering rich topological phenomena. Furthermore, we showed that the mean chiral displacement serves as a sensitive dynamical probe, effectively capturing the topological transitions and the presence of multiple TAI phases in the system. These

findings highlight the potential of photonic waveguide lattices for exploring disorder-induced topological effects and open new avenues for the design and manipulation of robust topological phases in engineered quantum systems.

Acknowledgments.—Z. X. is supported by the NSFC (Grant No. 12375016), and Beijing National Laboratory for Condensed Matter Physics (No. 2023BNL-CMPKF001). Y. Z. is supported by the NSFC (Grant No. 12474492 and No. 12461160324) and the Challenge Project of Nuclear Science (Grant No. TZ2025017). S. C. is supported by National Key Research and Development Program of China (Grant No. 2023YFA1406704), the NSFC under Grants No. 12174436 and No. T2121001 and the Strategic Priority Research Program of Chinese Academy of Sciences under Grant No. XDB33000000.

Data availability.—The data that support the findings of this article are not publicly available. The data are available from the authors upon reasonable request.

^{*} Corresponding author: ybzhang@zstu.edu.cn

[†] Corresponding author: schen@iphy.ac.cn

[‡] Corresponding author: xuzhihao@sxu.edu.cn

- ¹ L. Lu, J. D. Joannopoulos, and M. Soljačić, Topological photonics, *Nat. Photon.* **8**, 821 (2014).
- ² T. Ozawa, H. M. Price, A. Amo, N. Goldman, M. Hafezi, L. Lu, M. C. Rechtsman, D. Schuster, J. Simon, O. Zilberberg, and I. Carusotto, Topological photonics, *Rev. Mod. Phys.* **91**, 015006 (2019).
- ³ Y. E. Kraus, Y. Lahini, Z. Ringel, M. Verbin, and O. Zilberberg, Topological states and adiabatic pumping in quasicrystals, *Phys. Rev. Lett.* **109**, 106402 (2012).
- ⁴ M. Verbin, O. Zilberberg, Y. Lahini, Y. E. Kraus, and Y. Silberberg, Topological pumping over a photonic Fibonacci quasicrystal, *Phys. Rev. B* **91**, 064201 (2015).
- ⁵ S. Stützer, Y. Plotnik, Y. Lumer, P. Titum, N. H. Lindner, M. Segev, M. C. Rechtsman, and A. Szameit, Photonic topological Anderson insulators, *Nature(London)* **560**, 461 (2018).
- ⁶ J. Deng, H. Dong, C. Zhang, Y. Wu, J. Yuan, X. Zhu, F. Jin, H. Li, Z. Wang, H. Cai, C. Song, H. Wang, J. Q. You, and D.-W. Wang, Observing the quantum topology of light, *Science* **378**, 966 (2022).
- ⁷ P. St-Jean, V. Goblot, E. Galopin, A. Lemaitre, T. Ozawa, L. Le Gratiet, I. Sagnes, J. Bloch, and A. Amo, Lasing in topological edge states of a one-dimensional lattice, *Nat. Photon.* **11**, 651 (2017).
- ⁸ M. Parto, S. Wittek, H. Hodaei, G. Harari, M. A. Bandres, J. Ren, M. C. Rechtsman, M. Segev, D. N. Christodoulides, and M. Khajavikhan, Edge-mode lasing in 1D topological active arrays, *Phys. Rev. Lett.* **120**, 113901 (2018).
- ⁹ H. Zhao, P. Miao, M. H. Teimourpour, S. Malzard, R. El-Ganainy, H. Schomerus, and L. Feng, Topological hybrid silicon microlasers, *Nat. Commun.* **9**, 981 (2018).
- ¹⁰ T. Dai, A. Ma, J. Mao, Y. Ao, X. Jia, Y. Zheng, C. Zhai, Y. Yang, Z. Li, B. Tang, J. Luo, B. Zhang, X. Hu, Q. Gong, and J. Wang, A programmable topological photonic chip, *Nat. Mater.* **23**, 928 (2024).

¹¹ W. Wang, Z. Shen, Y. J. Tan, K. Chen, and R. Singh, On-chip topological edge state cavities, *Light Sci. Appl.* **14**, 330 (2025).

¹² X. Cheng, C. Jouvaud, X. Ni, S. H. Mousavi, A. Z. Genack, and A. B. Khanikaev, Robust reconfigurable electromagnetic pathways within a photonic topological insulator, *Nat. Mater.* **15**, 542 (2016).

¹³ K. Nomura and N. Nagaosa, Surface-quantized anomalous Hall current and the magnetoelectric effect in magnetically disordered topological insulators, *Phys. Rev. Lett.* **106**, 166802 (2011).

¹⁴ F. Evers and A. D. Mirlin, Anderson transitions, *Rev. Mod. Phys.* **80**, 1355 (2008).

¹⁵ H. L. Li, C.-Z. Chen, H. Jiang, and X. C. Xie, Coexistence of quantum Hall and quantum anomalous Hall phases in disordered MnBi₂Te₄, *Phys. Rev. Lett.* **127**, 236402 (2021).

¹⁶ E. Prodan, T. L. Hughes, and B. A. Bernevig, Entanglement spectrum of a disordered topological Chern insulator, *Phys. Rev. Lett.* **105**, 115501 (2010).

¹⁷ X. Cheng, H. Jiang, J. Chen, L. Zhang, Y. S. Ang, and C. H. Lee, Non-Hermitian effective \mathcal{PT} -symmetry restoration from structural disorder, *Front. Phys.* **21**, 035201 (2026).

¹⁸ S. S. Krishtopenko, M. Antezza, and F. Teppe, Disorder-induced topological phase transition in HgCdTe crystals, *Phys. Rev. B* **106**, 115203 (2022).

¹⁹ Y.-S. Hu, Y.-R. Ding, J. Zhang, Z.-Q. Zhang, and C.-Z. Chen, Disorder and phase diagrams of higher-order topological insulators, *Phys. Rev. B* **104**, 094201 (2021).

²⁰ H.-B. Wu and J.-J. Liu, Anderson disorder-induced non-trivial topological phase transitions in two-dimensional topological superconductors, *Phys. Rev. B* **103**, 115430 (2021).

²¹ Z.-Y. Ong and C. H. Lee, Transport and localization in a topological phononic lattice with correlated disorder, *Phys. Rev. B* **94**, 134203 (2016).

²² J. Song and E. Prodan, AIII and BDI topological systems at strong disorder, *Phys. Rev. B* **89**, 224203 (2014).

²³ A. Girschik, F. Libisch, and S. Rotter, Topological insulator in the presence of spatially correlated disorder, *Phys. Rev. B* **88**, 014201 (2013).

²⁴ C.-A. Li, B. Fu, Z.-A. Hu, J. Li, and S.-Q. Shen, Topological phase transitions in disordered electric quadrupole insulators, *Phys. Rev. Lett.* **125**, 166801 (2020).

²⁵ A. Chen, J. Maciejko, and I. Boettcher, Anderson localization transition in disordered hyperbolic lattices, *Phys. Rev. Lett.* **133**, 066101 (2024).

²⁶ J.-H. Wang, Y.-B. Yang, N. Dai, and Y. Xu, Structural-disorder-induced second-order topological insulators in three dimensions, *Phys. Rev. Lett.* **126**, 206404 (2021).

²⁷ C. Wang, T. Cheng, Z. Liu, F. Liu, and H. Huang, Structural amorphization-induced topological order, *Phys. Rev. Lett.* **128**, 056401 (2022).

²⁸ C. Grindall, A. C. Tyner, A.-K. Wu, T. L. Hughes, and J. H. Pixley, Separate surface and bulk topological Anderson localization transitions in disordered axion insulators, *Phys. Rev. Lett.* **135**, 226601 (2025).

²⁹ J. Li, R.-L. Chu, J. K. Jain, and S.-Q. Shen, Topological Anderson insulator, *Phys. Rev. Lett.* **102**, 136806 (2009).

³⁰ H. Jiang, L. Wang, Q.-F. Sun, and X. C. Xie, Numerical study of the topological Anderson insulator in HgTe/CdTe quantum wells, *Phys. Rev. B* **80**, 165316 (2009).

³¹ C. W. Groth, M. Wimmer, A. R. Akhmerov, J. Tworzydlo, and C. W. J. Beenakker, Theory of the topological Anderson insulator, *Phys. Rev. Lett.* **103**, 196805 (2009).

³² H.-M. Guo, G. Rosenberg, G. Refael, and M. Franz, Topological Anderson insulator in three dimensions, *Phys. Rev. Lett.* **105**, 216601 (2010).

³³ J. Song, H. Liu, H. Jiang, Q.-F. Sun, and X. C. Xie, Dependence of topological Anderson insulator on the type of disorder, *Phys. Rev. B* **85**, 195125 (2012).

³⁴ P. Titum, N. H. Lindner, M. C. Rechtsman, and G. Refael, Disorder-induced Floquet topological insulators, *Phys. Rev. Lett.* **114**, 056801 (2015).

³⁵ L.-Z. Tang, L.-F. Zhang, G.-Q. Zhang, and D.-W. Zhang, Topological Anderson insulators in two-dimensional non-Hermitian disordered systems, *Phys. Rev. A* **101**, 063612 (2020).

³⁶ W. Zhang, D. Zou, Q. Pei, W. He, J. Bao, H. Sun, and X. Zhang, Experimental observation of higher-order topological Anderson insulators, *Phys. Rev. Lett.* **126**, 146802 (2021).

³⁷ T. Peng, C.-B. Hua, R. Chen, D.-H. Xu, and B. Zhou, Topological Anderson insulators in an Ammann-Beenker quasicrystal and a snub-square crystal, *Phys. Rev. B* **103**, 085307 (2021).

³⁸ X. Cui, R.-Y. Zhang, Z.-Q. Zhang, and C. T. Chan, Photonic \mathbb{Z}_2 topological Anderson insulators, *Phys. Rev. Lett.* **129**, 043902 (2022).

³⁹ Q. Lin, T. Li, L. Xiao, K. Wang, W. Yi, and P. Xue, Observation of non-Hermitian topological Anderson insulator in quantum dynamics, *Nat. Commun.* **13**, 3229 (2022).

⁴⁰ X. Cheng, T. Qu, L. Xiao, S. Jia, J. Chen, and L. Zhang, Topological Anderson amorphous insulator, *Phys. Rev. B* **108**, L081110 (2023).

⁴¹ M. Ren, Y. Yu, B. Wu, X. Qi, Y. Wang, X. Yao, J. Ren, Z. Guo, H. Jiang, H. Chen, X.-J. Liu, Z. Chen, and Y. Sun, Realization of gapped and ungapped photonic topological Anderson insulators, *Phys. Rev. Lett.* **132**, 066602 (2024).

⁴² N. Sobrosa, M. Gonçalves, and E. V. Castro, Instability of quadratic band crossing systems to topological Anderson insulating phases, *Phys. Rev. B* **109**, 184206 (2024).

⁴³ B. D. Assunção, G. J. Ferreira, and C. H. Lewenkopf, Phase transitions and scale invariance in topological Anderson insulators, *Phys. Rev. B* **109**, L201102 (2024).

⁴⁴ Z.-W. Zuo, J.-R. Lin, and D. Kang, Topological inverse Anderson insulator, *Phys. Rev. B* **110**, 085157 (2024).

⁴⁵ E. J. Meier, F. A. An, A. Dauphin, M. Maffei, P. Massignan, T. L. Hughes, and B. Gadway, Observation of the topological Anderson insulator in disordered atomic wires, *Science* **362**, 929 (2018).

⁴⁶ G.-G. Liu, Y. Yang, X. Ren, H. Xue, X. Lin, Y.-H. Hu, H.-X. Sun, B. Peng, P. Zhou, Y. Chong, and B. Zhang, Topological Anderson Insulator in Disordered Photonic Crystals, *Phys. Rev. Lett.* **125**, 133603 (2020).

⁴⁷ S. Longhi, Topological Anderson phase in quasi-periodic waveguide lattices, *Opt. Lett.* **45**, 4036 (2020).

⁴⁸ G.-Q. Zhang, L.-Z. Tang, L.-F. Zhang, D.-W. Zhang, and S.-L. Zhu, Connecting topological Anderson and Mott insulators in disordered interacting fermionic systems, *Phys. Rev. B* **104**, L161118 (2021).

⁴⁹ L.-Z. Tang, S.-N. Liu, G.-Q. Zhang, and D.-W. Zhang, Topological Anderson insulators with different bulk states in quasiperiodic chains, *Phys. Rev. A* **105**, 063327 (2022).

⁵⁰ Z. Lu, Z. Xu, and Y. Zhang, Exact mobility edges and topological Anderson insulating phase in a slowly varying quasiperiodic model, *Ann. Phys.(Berlin)* **534**, 2200203 (2022).

⁵¹ X. Li, H. Xu, J. Wang, L.-Z. Tang, D.-W. Zhang, C. Yang, T. Su, C. Wang, Z. Mi, W. Sun, X. Liang, M. Chen, C. Li, Y. Zhang, K. Linghu, J. Han, W. Liu, Y. Feng, P. Liu, G. Xue, J. Zhang, Y. Jin, S.-L. Zhu, H. Yu, S. P. Zhao, and Q.-K. Xue, Mapping the topology-localization phase diagram with quasiperiodic disorder using a programmable superconducting simulator, *Phys. Rev. Res.* **6**, L042038 (2024).

⁵² X.-M. Wang, S.-Z. Li, and Z. Li, Emergent topological re-entrant phase transition in a generalized quasiperiodic modulated Su-Schrieffer-Heeger model, *Phys. Rev. A* **111**, 022214 (2025).

⁵³ A. Sinha, T. Shit, A. Tetarwal, D. Sen, and S. Mukherjee, Probing the topological Anderson transition in quasiperiodic photonic lattices via chiral displacement and wavelength tuning, *Phys. Rev. A* **112**, 013512 (2025).

⁵⁴ S.-N. Liu, G.-Q. Zhang, L.-Z. Tang, and D.-W. Zhang, Topological Anderson insulators induced by random binary disorders, *Phys. Lett. A* **431**, 128004 (2022).

⁵⁵ A. K. Ghosh, T. Nag, and A. Saha, Floquet second-order topological Anderson insulator hosting corner localized modes, *Phys. Rev. B* **110**, 125427 (2024).

⁵⁶ R. Ji and Z. Xu, Fibonacci-modulation-induced multiple topological Anderson insulators, *Commun. Phys.* **8**, 336 (2025).

⁵⁷ I. C. Fulga, F. Hassler, A. R. Akhmerov, and C. W. J. Beenakker, Scattering formula for the topological quantum number of a disordered multimode wire, *Phys. Rev. B* **83**, 155429 (2011).

⁵⁸ I. Mondragon-Shem, T. L. Hughes, J. Song, and E. Prodan, Topological criticality in the chiral-symmetric AIII class at strong disorder, *Phys. Rev. Lett.* **113**, 046802 (2014).

⁵⁹ D. Christodoulides, F. Lederer, and Y. Silberberg, Discretizing light behaviour in linear and nonlinear waveguide lattices, *Nature* **424**, 817 (2003).

⁶⁰ S. Longhi, Quantum-optical analogies using photonic structures, *Laser Photon. Rev.* **3**, 243 (2009).

⁶¹ I. L. Garanovich, S. Longhi, A. A. Sukhorukov, and Y.

S. Kivshar, Light propagation and localization in modulated photonic lattices and waveguides, *Phys. Rep.* **518**, 1 (2012).

⁶² G. Corrielli, G. Della Valle, A. Crespi, R. Osellame, and S. Longhi, Observation of surface states with algebraic localization, *Phys. Rev. Lett.* **111**, 220403 (2013).

⁶³ Z. Lu, Y. Zhang, and Z. Xu, Reentrant localization transitions in a topological Anderson insulator: A study of a generalized Su-Schrieffer-Heeger quasicrystal, *Front. Phys.* **20**, 024204 (2025).

⁶⁴ F. Cardano, A. D'Errico, A. Dauphin, M. Maffei, B. Piccirillo, C. de Lisio, G. De Filippis, V. Cataudella, E. Santamato, L. Marrucci, M. Lewenstein, and P. Massignan, Detection of Zak phases and topological invariants in a chiral quantum walk of twisted photons, *Nat. Commun.* **8**, 15516 (2017).

End Matter

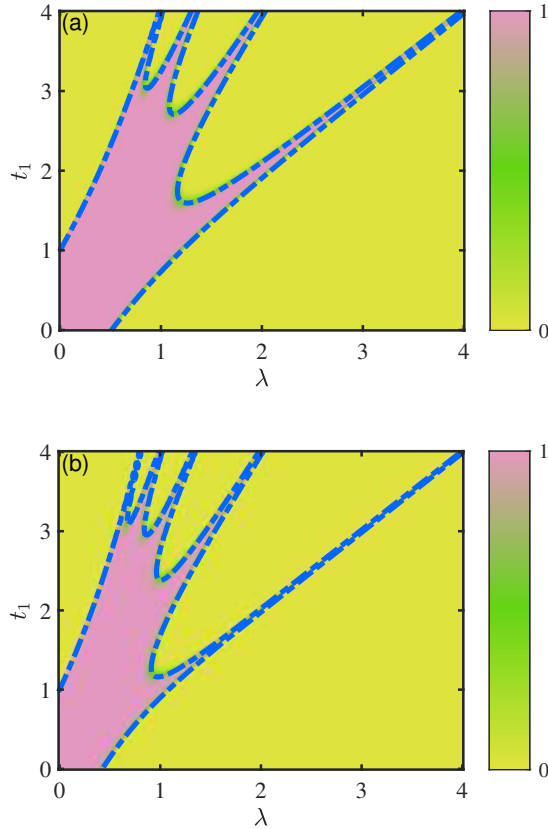


FIG. A1: The disorder-average topological phase diagram as a function of the intradimer hopping amplitude t_1 and the disorder strength λ for (a) $\xi^{(m)} = m\lambda$, ($m = 1, 2, 3, 4$), $p_1 = 7/20$, $p_2 = 1/4$, $p_3 = p_4 = 1/5$ and (b) $\xi^{(m)} = m\lambda$, ($m = 1, 2, 3, 4, 5$), $p_1 = p_2 = 1/4$, $p_3 = p_4 = p_5 = 1/6$. The blue dashed lines correspond to the topological phase boundaries. Here, all the data are averaged by $N_c = 200$ disorder realizations.

Appendix: Cases of Multivariate distributions.—To further elucidate how the number of disorder components M affects the emergence of TAI phases, we present disorder-averaged topological phase diagrams as functions of t_1 and λ for $M = 4$ and $M = 5$ in Fig. A1. For $M = 4$, the disorder is defined as $\xi^{(m)} = m\lambda$ ($m = 1, 2, 3, 4$), with probabilities $p_1 = 7/20$, $p_2 = 1/4$, and $p_3 = p_4 = 1/5$. For $M = 5$, we use $\xi^{(m)} = m\lambda$ ($m = 1, 2, 3, 4, 5$), occurring with probabilities $p_1 = p_2 = 1/4$ and $p_3 = p_4 = p_5 = 1/6$. As shown in Fig. A1, the overall phase diagram structure is consistent with the cases for $M = 2$ and 3. Crucially, in the regime of large t_1 , the number of distinct TAI phase emergences matches exactly the value of M : for $M = 4$, four TAI phase appear, and for $M = 5$, five TAI phases are observed. This one-to-one correspondence demonstrates that the complexity of the disorder directly determines the number of TAI intervals, providing a precise and versatile mechanism to control the topological phase landscape. These results highlight the power of multivariate disorder as a tunable tool for engineering multiple, customizable TAI phases in photonic and quantum systems.